Optica Imaging Congress 2025 (3D, COSI, DH, IS, pcAOP, RadIT) © Optica Publishing Group 2025

Data-driven Stochastic Wavefront Optimization for Multispectral Extended Depth-of-Field Imaging

Exequiel Oliva,[1] Nelson Díaz[1], Samuel Pinilla [2] and Esteban Vera [1,*]

[1] School of Electrical Engineering, Pontificia Universidad Católica de Valparaíso, Chile
[2] Rutherford Appleton Laboratory, Science and Technology Facilities Council, Harwell, UK

[*] esteban.vera@pucv.cl

Abstract: This work presents a multispectral-aware diffractive optical element design for extended depth-of-field imaging. By using a data-driven stochastic optimization approach, the proposed method enhances spectral fidelity and depth invariance, outperforming state-of-the-art methods.

1. Introduction

Depth-of-field (DoF) refers to the image region where objects appear in focus. Increasing DoF typically reduces light intake, which limits performance in multispectral systems. Wavefront coding (WC) addresses this by introducing recoverable blur, commonly implemented through diffractive optical elements (DOEs) [1]. While recent end-to-end (E2E) [2] and hardware-in-the-loop (HIL) [3] approaches have improved DOE design, multispectral applications remain challenging. This work proposes a novel DOE design for multispectral extended DoF using the covariance matrix adaptation evolution strategy (CMA-ES) optimization with a parametric model combining cubic phase masks and Zernike polynomials, all within a simulation framework.

2. Method

We propose a computational framework for designing and optimizing a DOE capable of enhancing multispectral EDoF imaging, which is depicted in Fig. 1. The proposed system is based on a simulated optical acquisition framework in which a DOE modulates the phase of the incident wavefront, influencing image formation across different spectral bands and depths. The DOE phase $h_\lambda(s,t)$ is parameterized as a combination of two fundamental components: the Cubic Phase [1] and the first 14 Zernike polynomials (excluding piston), then $h_\lambda(s,t) = \alpha(s^3 + t^3) + \Sigma_{p=1}^{P} \rho_p Z_p(s,t)$, where $Z_p(s,t)$ are the p^{th} Zernike Polynomial with coefficient ρ_p to be estimated, and α is the cubic phase coefficient controlling the WC, P is the number of Zernike polynomials. Thus, the full set of DOE parameters to be optimized is $\Theta_{DOE} = (\alpha, \rho_1, \ldots, \rho_P)$.

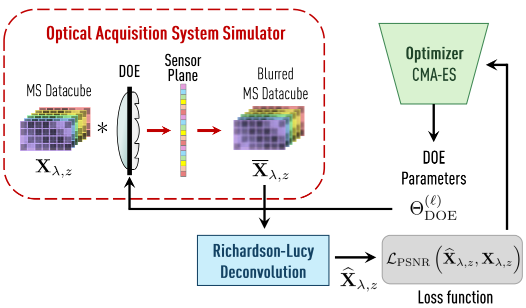

Fig. 1. Overview of the computational framework used for optimizing the DOE.

The discrete mathematical model governing the optical system can be expressed as $\overline{\mathbf{X}}_{\lambda,z} = \mathbf{PSF}_{\lambda,z} * \mathbf{X}_{\lambda,z} + \Omega_{\lambda,z}$, where $\mathbf{PSF}_{\lambda,z}$ is the wavelength-depth PSF, z is the scene depth, λ is the wavelength of the spatially incoherent ligth, $\mathbf{X}_{\lambda,z}$ is the wavelength-depth dependent scene, $\overline{\mathbf{X}}_{\lambda,z}$ is the blurred multispectral image and $\Omega_{\lambda,z} \sim \mathcal{N}(0, \sigma_s^2)$ is a zero-mean Gaussian noise with standard deviation σ_s.

3. Simulation Results

To assess the performance of the optimized DOE, we conducted an evaluation using the CAVE dataset, which have 32 multispectral scenes, with a spatial resolution of 512×512 and 31 spectral bands, with a spectral resolution of 10 $[nm]$ between 400 $[nm]$ and 700 $[nm]$. In order to measure the spatial fidelity, we use the PSNR and SSIM, where high values of PSNR and SSIM denote better spatial accuracy. Moreover, we use the SAM to test the spectral fidelity, where lower SAM metrics stands for better spectral similarity. The proposed DOE phase was compared against three state-of-the-art (SOTA) approaches, the classic cubic phase mask [1], an end-2-end DOE optimization (E2E, [4]), and a hardware-in-the-loop DOE optimization (HIL, [3]).

			DOE			
Metrics	Depth $[m]$	Refractive lens only	Cubic [1]	HIL [3]	E2E [4]	Proposed
PSNR	$z = 0.5$	$29.0287 \pm \mathbf{3.7285}$	35.2548 ± 5.0672	31.3922 ± 5.0367	31.6781 ± 3.9104	$\mathbf{36.4552} \pm 5.7208$
	$z = 1.0$	$32.3221 \pm \mathbf{3.9806}$	36.0219 ± 5.9079	33.6696 ± 5.3771	35.1609 ± 4.9382	$\mathbf{38.0425} \pm 6.1682$
	$z = 2.0$	$33.5484 \pm \mathbf{4.5712}$	36.8269 ± 6.0360	34.9550 ± 5.5430	35.4093 ± 5.4663	$\mathbf{38.7882} \pm 5.7744$
	$z = \infty$	$34.7331 \pm \mathbf{5.3382}$	37.5607 ± 6.0382	35.2440 ± 5.5071	34.4859 ± 5.4032	$\mathbf{38.4501} \pm 5.8608$
	Average	$32.4081 \pm \mathbf{3.9165}$	36.4161 ± 5.6579	33.8152 ± 5.0958	34.1836 ± 4.4568	$\mathbf{37.9340} \pm 5.7763$
SSIM	$z = 0.5$	0.9060 ± 0.0524	0.9598 ± 0.0231	0.9308 ± 0.0399	0.9320 ± 0.0355	$\mathbf{0.9640} \pm \mathbf{0.0191}$
	$z = 1.0$	0.9480 ± 0.0301	0.9630 ± 0.0228	0.9608 ± 0.0191	0.9668 ± 0.0202	$\mathbf{0.9725} \pm \mathbf{0.0148}$
	$z = 2.0$	0.9598 ± 0.0242	0.9660 ± 0.0214	0.9679 ± 0.0151	0.9574 ± 0.0230	$\mathbf{0.9761} \pm \mathbf{0.0118}$
	$z = \infty$	0.9645 ± 0.0213	0.9684 ± 0.0194	0.9674 ± 0.0164	0.9528 ± 0.0237	$\mathbf{0.9761} \pm \mathbf{0.0113}$
	Average	0.9446 ± 0.0312	0.9643 ± 0.0216	0.9567 ± 0.0218	0.9498 ± 0.0240	$\mathbf{0.9722} \pm \mathbf{0.0140}$
SAM	$z = 0.5$	0.1504 ± 0.0483	0.1135 ± 0.0472	0.1459 ± 0.0499	0.1304 ± 0.0470	$\mathbf{0.1077} \pm \mathbf{0.0446}$
	$z = 1.0$	0.1270 ± 0.0530	0.1071 ± 0.0459	0.1187 ± 0.0492	0.1222 ± 0.0517	$\mathbf{0.1008} \pm \mathbf{0.0440}$
	$z = 2.0$	0.1149 ± 0.0527	0.1053 ± 0.0459	0.1098 ± 0.0484	0.1211 ± 0.0540	$\mathbf{0.0995} \pm \mathbf{0.0447}$
	$z = \infty$	0.1111 ± 0.0516	0.1052 ± 0.0462	0.1129 ± 0.0498	0.1233 ± 0.0518	$\mathbf{0.1008} \pm \mathbf{0.0462}$
	Average	0.1259 ± 0.0508	0.1078 ± 0.0463	0.1218 ± 0.0489	0.1243 ± 0.0509	$\mathbf{0.1022} \pm \mathbf{0.0448}$

Table 1. Spatial and spectral quantitative comparison between a normal refractive lens, the addition of three state-of-the-art DOEs and our proposed DOE design using averaged PSNR, SSIM, and SAM metrics obtained with the Cave dataset.

The average values obtained for the PSNR, SSIM and SAM across the entire dataset are summarized in Table 3. These results provide a comprehensive assessment of the spectral and spatial fidelity of each DOE design, confirming the superior performance of the proposed phase profile. The proposed DOE consistently outperforms the other designs across all three metrics, achieving the highest PSNR and SSIM, along with the lowest SAM. The only caveat is that the PSNR values for the designed DOE have more variability, perhaps proportional to the larger PSNR values achieved. These values indicate that the proposed phase achieves the best balance between structural similarity and spectral fidelity.

4. Conclusion

We successfully introduced a multispectral EDoF imaging system using a stochastic wavefront optimization approach. By optimizing a DOE using a simulation framework inspired by the HIL approach, we were able to find the optimal mixture between a cubic phase mask and a set of Zernike coefficients for enhanced spectral performance with an extended depth-of-field. Our results demonstrate that the optimized DOE enhances both spatial-spectral fidelity and DoF. The proposed approach surpasses in PSNR all the other DOE designs for all reconstructed depths, leading to a global average advantage of nearly 2dB, while also steadily delivering the best SSIM and SAM metrics.

References

1. E. R. Dowski and W. T. Cathey, "Extended depth of field through wave-front coding," *Appl. Opt.*, vol. 34, no. 11, pp. 1859–1866, Apr 1995. [Online]. Available: https://opg.optica.org/ao/abstract.cfm?URI=ao-34-11-1859
2. V. Sitzmann, S. Diamond, Y. Peng, X. Dun, S. Boyd, W. Heidrich, F. Heide, and G. Wetzstein, "End-to-end optimization of optics and image processing for achromatic extended depth of field and super-resolution imaging," *ACM Transactions on Graphics (TOG)*, vol. 37, no. 4, pp. 1–13, 2018.
3. S. Pinilla, S. R. Miri Rostami, I. Shevkunov, V. Katkovnik, and K. Egiazarian, "Hybrid diffractive optics design via hardware-in-the-loop methodology for achromatic extended-depth-of-field imaging," *Optics Express*, vol. 30, no. 18, pp. 32 633–32 649, 2022.
4. U. Akpinar, E. Sahin, M. Meem, R. Menon, and A. Gotchev, "Learning wavefront coding for extended depth of field imaging," *IEEE transactions on image processing*, vol. 30, pp. 3307–3320, 2021.